

UCRL-JRNL-208844

# Radiative and Dynamical Feedbacks Over the Equatorial Cold-Tongue: Results from Seven Atmospheric GCMs

D.-Z. Sun, T. Zhang, C. Covey, S. Klein, W. Collins, J. Kiehl, J. Meehl, I. Held, M. Suarez

January 5, 2005

Journal of Climate

## Disclaimer

# Radiative and Dynamical Feedbacks Over the Equatorial Cold-Tongue: Results from Seven Atmospheric GCMs

D.-Z. Sun and T. Zhang
Climate Diagnostics Center, NOAA-CIRES

C. Covey and S. Klein
Lawrence Livermore National Laboratory

W.Collins, J. Kiehl, and J. Meehl
National Center For Atmospheric Research

I. Held
Geophysical Fluid Dynamics Laboratory, NOAA

M. Suarez
National Aronics and Space Administration

January 1, 2005

## Abstract

The equatorial Pacific is a region with strong negative feedbacks. Yet coupled GCMs have exhibited a propensity to develop a significant SST bias in that region, suggesting an unrealistic sensitivity in the coupled models to small energy flux errors that inevitably occur in the individual model components. Could this "hypersensitivity" exhibited in a coupled model be due to an underestimate of the strength of the negative feedbacks in this region? With this suspicion, the feedbacks in the equatorial Pacific in seven atmospheric GCMs (AGCMs) have been quantified using the interannual variations in that region and compared with the corresponding calculations from the observations. The seven AGCMs are: the NCAR CAM1, the NCAR CAM2,the NCAR CAM3, the NASA/NSIPP Atmospheric Model, the Hadley Center Model, the GFDL AM2p10, and the GFDL AM2p12. All the corresponding coupled runs of these seven AGCMs have an excessive cold-tongue in the equatorial Pacific.

The net atmospheric feedback over the equatorial Pacific in the two GFDL models is found to be comparable to the observed value. All other models are found to have a weaker negative net feedback from the atmosphere—a weaker regulating effect on the underlying SST than the real atmosphere. A weaker negative feedback from the cloud albedo and a weaker negative feedback from the atmospheric transport are the two leading contributors to the weaker regulating effect from the model atmosphere. All models overestimate somewhat the positive feedback from water vapor. These results confirm the suspicion that an underestimate of negative feedbacks from the atmosphere over the equatorial Pacific region is a prevalent problem. The results also suggest, however, that a weaker regulatory effect from the atmosphere is unlikely solely responsible for the "hypersensitivity" in all models. The need to validate the feedbacks from the ocean transport is therefore highlighted.

# 1.Introduction

The equatorial Pacific is a region with strong negative feedbacks. Ramanathan and Collins (1991) first observed that a SST anomaly in the central Pacific triggers a negative response from clouds—clouds reflect more (less) solar radiation back to space in response to a positive (negative) SST changes. They even postulated that this negative feedback of cloud albedo may be a "thermostat" of the tropics. Subsequent studies point out the importance of the feedbacks from the atmospheric and oceanic dynamics (Fu et al 1990, Wallace 1992, Pierrehumert 1995, Sun and Liu 1996). In an attempt to assess the relative importance of the cloud albedo feedback and the feedback from dynamics, Sun and Trenberth (1998) used the best data available and quantified the changes in the heat transport in the atmosphere and in the ocean associated with the 1986-87 El Niño warming in addition to calculating the changes in the radiative fluxes. The results show that the negative feedback from the cloud albedo is actually a smaller player compared to the other two negative feedbacks in the equatorial Pacific region, namely the feedback from the heat transport by the atmospheric circulation and the feedback from the poleward heat transport by the ocean circulation. The negative feedback from the poleward ocean heat transport is found to be twice as strong as the negative feedback from the atmospheric transport. The latter is in turn twice as strong as the cloud albedo feedback. Against this background, the prevalence of a profound bias in the central equatorial Pacific in coupled GCMs is a surprise. To be sure, the lack of phytoplankton in the model ocean could lead to an underestimate of the solar radiation absorbed by the ocean (Murtugudde et al. 2002). The lack of sufficient vertical resolution of the ocean model may also lead to an excessive cooling of the surface ocean (Stockdale et al. 1998). However, the fact that the excessive cold-tongue is mostly

a problem of coupled models suggest that the errors in the energy fluxes in the individual components of the coupled model are small. The question that is particularly puzzling to us is that given the existence of a myriad of strong negative feedbacks, why the SST in this region, when simulated by a coupled model, appears to be sensitive to small flux errors in the model components? Could it be that the strength of one or more negative feedbacks in the model underestimated? Or alternatively, could it be that the strength of one or more positive feedbacks in the model is overestimated?

A preliminary attempt to answer these questions was made by Sun et al. (2003). By examining the response of radiative and dynamical fluxes to ENSO in the NCAR CCM3, they noted that the negative feedback of cloud albedo is substantially underestimated in the model. In further light of some coupled experiments, they put forward the hypothesis that a weaker regulating effect from the atmosphere may be a significant contributor to the development of an excessive cold-tongue in the corresponding coupled model. The purpose of this study is to extend the same analysis to six additional models whose corresponding coupled runs also have an excessive cold-tongue in the equatorial Pacific. The almost ubiquitous presence of an excessive cold-tongue in the equatorial Pacific in the coupled GCMs offers a unique opportunity to understand the causes for this syndrome: a hypothesis developed in one model can be readily tested against other models.

## 2. Methods

The study employs the same method of Sun et al. (2003). We use the surface warming associated with El Niño as the forcing signal. We will then examine how radiative fluxes at the top of the

atmosphere (TOA) and the vertically integrated transport of energy in the atmosphere vary in relation to the underlying SST. We quantify the feedbacks by regressing the corresponding fluxes to the SST.

The cloud and water vapor feedbacks in this paper are measured in the same way as that of Cess and Potter (1988): water vapor feedback is equated with the change in the greenhouse effect in the clear sky region, and the cloud feedbacks are equated with the corresponding changes in the long-wave and short-wave cloud forcing. These measures are not the same as the measures of Wetherald and Manabe (1988) which use offline radiative transfer calculations to obtain the true partial derivatives (Soden et al. 2004). The measures of Cess and Potter (1988) tend to overestimate the feedback from the greenhouse effect of water vapor and underestimate the feedback from the greenhouse effect of clouds. However, provided the feedbacks in the models are measured in the same way as in the observations, the errors revealed in the analysis are still true errors in the models. The available radiation data measure the feedbacks of water vapor and clouds on the ENSO time-scale in the form of Cess and Potter (1988). Also, the concern here is more with the combined effect of water vapor and cloud feedbacks on the response in the net surface heat flux into the ocean—the net atmospheric feedback—than with the accuracy in the definition of individual feedbacks of water vapor and clouds, the distinctions between the measures of Cess and Portter (1988) and Wetherald and Manabe (1988) of the individual feedbacks of water vapor and clouds are considered less important.

The observational data comes from ERBE (Barkstrom et al. 1989) and the NCEP reanalysis (Trenberth et al. 2001). The model data are from the AMIP runs over the ERBE period. The

AMIP runs have the observed, time-varying SST as the boundary conditions. Therefore, the model atmosphere is subject to the same SST forcing as the real atmosphere.

The models that have been analyzed include (1) the NCAR CAM1 (Kiehl et al. 1998), (2) the NCAR CAM2 (Collins et al. 2003), (3) the NCAR CAM3 (Collins et al. 2004), (4) the NASA NSIPP model (Chou and Suarez 1996, Suarez 1995), (5) the Hadley Center Model (Collins et al. 2001), (6) the GFDL AM2p10, and (7) the GFDL AM2p12 (Anderson et al. 2004). ( The GFDL AM2p10 is an earlier version of the GFDL AM2p12. The main differences between the two versions are in the use of boundary layer schemes and in the vertical layers. The AM2p10 uses the boundary layer scheme of Mellor and Yamada (1974) while the AM2p12 uses the boundary layer scheme of Lock et al. (2000). The AM2p12 has 24 vertical layers while the AM2p10 has 18 vertical layers).

The seven models involve the use of four different schemes for most convection. The NCAR models use the deep convection scheme by Zhang and McFarlane (1995) and the shallow convection scheme by Hack (1994). The NASA NSIPP model and the two GFDL models use the Relaxed Arakawa Schubert (RAS) scheme (Moorthi and Suarez 1992). The Hadley Center model uses a mass-flux scheme (Gregory 1990, Gregory and Rowntree 1990) that is based on the bulk cloud model of Yanai et al. (1973). The seven models also have different vertical and horizontal resolutions. The vertical resolutions vary from 18 layers (NCAR CAM1) to 34 layers (NASA NSIPP). The horizontal resolutions vary from about $3.8^{o}X2.5^{o}$ in the Hadley Centre model to $2.5^{o}X2.0^{o}$ in the GFDL and the NASA models. Despite the many differences in these seven atmosphere models, gauged by the meridional and zonal SST gradients over the equatorial

Pacific, all their corresponding coupled models have an excessive cold-tongue over the central equatorial Pacific (Fig. 1).

## 3. Results

The estimates of the feedbacks from these models over the central equatorial Pacific region (150°E-250°E, 5°S-5°N) are summarized in Table 1. The definition of the symbols and the procedure of the calculations are the same as in Sun et al. (2003). $\frac{\partial}{\partial T} G_a$ is the water vapor feedback, $\frac{\partial}{\partial T} C_l$ is the feedback from the greenhouse effect of clouds, $\frac{\partial}{\partial T} C_s$ is the feedback from the short-wave forcing of clouds, and $\frac{\partial}{\partial T} D_a$ is the feedback from the atmospheric transport. $\frac{\partial F_a}{\partial T} = \frac{\partial G_a}{\partial T} + \frac{\partial C_l}{\partial T} + \frac{\partial C_s}{\partial T} + \frac{\partial D_a}{\partial T}$ and is termed as the net atmospheric feedback. $\frac{\partial}{\partial T} F_s$ is the feedback from net surface heat flux into the ocean. Neglecting the heat storage in the atmosphere, which is small (Sun 2000), $\frac{\partial}{\partial T} F_s$ differs $\frac{\partial}{\partial T} F_a$ by a constant—the rate of change of the ocean's surface emission with respect to SST.

With the exception of the two GFDL models, all other models underestimate the negative feedback from the cloud albedo and the negative feedback from the atmospheric transport. The underestimate in the cloud albedo appears to be particularly worrisome as this feedback in one of these models has the opposite sign of the observed. The NCAR CAM2 differs from the observed value in its simulation of the cloud albedo feedback by as much as 12.8 W/m$^2$/K. With the exception of the two GFDL models, the underestimate of the strength of the negative feedback from the atmospheric transport in these models are also significant. The error ranges from 4.6

$W/m^2/K$ in the Hadley Center model to 7.7 $W/m^2/K$ in the NCAR CAM3. All models overestimate the positive feedback from water vapor. The error ranges from 15%--50%. The GFDL AM2p10 has the smallest error in the simulation of the water vapor feedback while the largest error is found in the Hadley Center model. Models also error on the estimate of the feedback from the long-wave forcing of clouds, but they do not bias toward the same direction. While the NCAR CCM3 (CAM1) overestimates the feedback from the long-wave forcing of clouds by 3.7 $W/m^2/K$, the NCAR CAM2 underestimates this feedback by 5.6 $W/m^2/K$. The underestimate of the feedback from the long-wave forcing of clouds in the Hadley Centre model is also large (4.6 $W/m^2/K$). The underestimate of the positive feedback from the long-wave forcing of clouds in the NCAR CAM2, the NCAR CAM3, the NASA NSIPP model, and the Hadley Centre model alleviates the effect of the errors on the net atmospheric feedback from the underestimate of the cloud albedo feedback and the overestimate of the water vapor feedback.

Because of the underestimate of the negative feedbacks from the cloud short-wave forcing and the atmospheric transport and to a less degree because of the overestimate of the positive feedback from water vapor, the negative net atmospheric feedback in all other models except the two GFDL models is underestimated over the region of concern. The results confirm the suspicion that underestimating the strength of the negative feedbacks in the region of concern is a prevalent problem in the climate models. The results from the GFDL models, however, are very encouraging. The net atmospheric feedback in the two GFDL models is comparable to the observed value. The improvements in the GFDL AM2p10 are not just from the improvements in the cloud albedo feedback, but from the improvements in the feedback from the atmospheric transport. In fact, the simulation of all the individual feedbacks in the GFDL AM2p10 is closer

to their corresponding observational estimate than the other models considered here. This suggests that there may be one key process that the model needs to have it right. Once this process is better estimated, simulation of other related processes then follows.

The horizontal pattern of the response in $G_a$ to ENSO forcing from the models show remarkable agreement with each other and with observations. Within the region of concern, the response of $G_a$ in the models is greater than in the real world grid-point by grid-point (Fig. 2). It is therefore tempting to suggest that the overestimate of $\frac{\partial}{\partial T} G_a$ in the equatorial Pacific in the models is because these models are still too diffusive in the vertical (Sun and Held 1996). It is interesting to note, however, that the AM2p12 overestimates $\frac{\partial}{\partial T} G_a$ more than the AM2p10 does even though the latter is a version that has fewer vertical levels. Ingram (2002) also noted that the increases in the vertical resolution in the models do not result in a weaker water vapor feedback. Four different cumulus parameterization schemes are used in the models analyzed here. The overestimate of the water vapor feedback in all models is thus particularly puzzling. One thing that all the four parameterization schemes lack is the inclusion of the effect of sub-grid scale variability. Whether the neglect of the effect of sub-grid scale variability makes the model atmosphere appear to be more "diffusive" emerges as a question of interest. The difference in the value of $\frac{\partial}{\partial T} G_a$ between the two versions of the GFDL model raises another question of potential interest: why the water vapor feedback in the model appears to be sensitive to the use of different boundary layer schemes?

While the spatial patterns of the response of $G_a$, in different models are strikingly similar, there is more variability in the response of $C_l$ (Fig.3). The NASA model is particularly notable--the

response of $C_l$ in the equatorial central Pacific near the dateline (180°E-140°W) is much weaker than the observed (Fig. 3e). This equatorial minimum response splits the response of $C_l$ to El Nino warming into two parts, each of which has a maximum off the equator. The response of $C_s$ and the rainfall in the NASA NSIPP model also has this "split pea" feature (Fig.4e and Fig.5e), indicating a lack of response of convection in the central equatorial Pacific near the date line in the model. The lack of response of $D_a$ in the same region in the NASA model (Fig. 6e) also suggests a lack of response of convection in the central equatorial Pacific.

Contrasting the spatial patterns in the response of the cloud forcing (Fig.3 and Fig.4) with the spatial patterns in the rainfall (Fig.5) confirms the impression that the leading source of errors in the response of $C_s$ may still be the most obvious: errors in the response of convection. The rainfall responses in the equatorial central Pacific in the CAM2 and the CAM3 are the two weakest, so are their responses in $C_s$. The improvement in the response in $C_s$ in the Hadley center and the GFDL model apparently follows the improvement in the response of convection. However, the response of convection in the model does not have the same control over the response of $C_l$: the Hadley Center model has a response in rainfall that is comparable to observations, the response in $C_l$ in the same model is only half of the value from observations. Convection also has a less control over the response in $G_a$. For example, the rainfall in the NCAR CAM2 and CAM3 is much weaker than that in CAM1, the response in $G_a$ in the NCAR CAM2 and CAM3 is only slightly weaker than that in CAM1.

The three NCAR models and the NASA model are the models that have a poor simulation of the response in $D_a$. The main problem with these models in their simulation of the response of $D_a$ is

lack of response on the equator near the date line region. The maximum response is located off equator in these four models. These four models also have the poorest simulation of the response of $C_s$. Interestingly, in the NCAR models, there does not appear to be a distinct lack of response in precipitation over the central equatorial Pacific where there is a distinct lack of response in $D_a$. The responses in the precipitation in the NCAR CAM2 and the NCAR CAM3, however, are weak throughout the concerned region (Fig. 5c, d), which is consistent with the much weak negative feedback from the atmospheric transport in the model shown in Table 1.

The impact of the errors in the aforementioned feedbacks on the response of the net surface heating ($F_s$) is further shown in Fig. 7, which gives a basin-wide, and a more critical view of the response of the model atmosphere. In four of the seven models (the NCAR CAM1, CAM2, CAM3, and the NASA NSIPP, the response of the surface heating to El Nino warming in the equatorial central Pacific (160$^o$E-140$^o$W) has the wrong sign. The response of $F_s$ in the Hadley Center model in the same region is near zero. The two GFDL models have adequate responses in the equatorial central Pacific. One of them—the GFDL AM2p10-- suffers a significant deficiency in the region east to about 120$^o$W. The negative response in the GFDL AM2p10 also does not extend as far west as in the observations. The zonal extent of the response in the later version of the GFDL model—the AM2p12—is improved, but the meridional extend of the response is more confined. Still, the spatial pattern of the response of $F_s$ in both the GFDL models resembles the observed remarkably well.

Diagnosing the root causes of all the model deficiencies is beyond the scope of the present paper and may require more sophisticated tools than simple regression analysis here. The encouraging

part of the present analysis is that it may not be a difficult task to have all the feedbacks right: the GFDL AM2p10 provides an example. Whether this good agreement between the simulations by the GFDL model and the observations is simply a luck or truly reflecting the fidelity of the model to Nature needs to be further examined. The better agreement in the spatial pattern of all the terms in the energy equation between the simulations by the GFDL AM2p10 and the observations suggest that something critical has been done right with this model. With the exception of the water vapor feedback, the improvements in the GFDL AM2p10 in the simulation of the feedbacks appear to be stable to changes in the vertical resolution and the boundary layer scheme. In any case, detailed diagnostic analysis of the differences between GFDL AM2p10 and other models could provide more information on why the GFDL AM2p10 got the feedbacks right and why other models are more distant from the targets.

## 4. Discussion

On one hand, the results from this analysis highlight that it remains a difficult issue to simulate the cloud and water vapor feedbacks over the equatorial Pacific by GCMs. Consistent with earlier analyses, the errors in the cloud feedbacks are most protruding. The errors in the water vapor feedback are also significant to call for renewed attention to the issue of water vapor feedback.

The concern with the cloud and water vapor feedback in the GCM is hardly new. What's surprising from this analysis is that the majority of models tend to bias towards the same direction in their simulations of the negative feedbacks in this region, namely, the short-wave cloud forcing and the negative feedback from the atmospheric transport. Equally interesting is

that the models also bias in the same direction in their simulation of the positive feedback from water vapor. In fact, there is even more consistency with the simulation of the water vapor feedback—all models overestimate the positive feedback from water vapor. The tendency for atmospheric models to overestimate the water vapor feedback has been noted before (Sun and Held 1996, Sun et al. 2001) with the use of rawinsonde data. It is reassuring to see that satellite data reveal the same tendency. Consistency among models is not a good argument for the fidelity of the models to Nature. In the same vein, given the tendency of models to bias towards the same direction, averaging over these models does not help with the reduction of the bias. The results thus caution the use of the spread among models in their prediction of global warming as the true bound of the uncertainty in predictions by the models. To be sure, the number of models analyzed there is still limited.

Another suggestion from this analysis is that bias in the atmospheric feedback is unlikely the sole cause of the excessive cold-tongue in the central equatorial Pacific. The simulation of the atmospheric feedbacks in the GFDL AM2p10 is probably as close to the observed as one has reasonably hoped, the corresponding coupled model still has an excessive cold-tongue (Fig. 1g). The results highlight the need to look at the ocean feedbacks. In light of the estimate of the relative importance of the feedbacks from the atmospheric transport and the feedback from the ocean transport by Sun and Trenberth (1998), the suggestion from the present analysis of an important role of the ocean transport is not surprising, but reassuring. Whether the ocean feedback in the coupled models is accurately estimated needs to be further examined. One way to do so is to check the response of the surface wind stress to changes in the SST and then the response of the ocean heat transport to the changes in the wind stress. The former can be

assessed to some degree using the AMIP runs of the atmospheric GCMs. The obstacle for carrying out this analysis immediately is the lack of good data for the tropical wind stress. The limited satellite data (Liu 2002) has revealed severe deficiencies in the NCEP reanalysis, but the satellite data are still too short for calculating feedbacks. The latter requires forced ocean experiments from different groups using the same surface forcing. These forced ocean model experiments are not yet available on the scale of the AMIP experiments. Nor is it clear whether the accuracy of ocean heat transport data is sufficient to validate the results from the model experiments.

Related to the assessment of the feedback from the ocean heat transport is the issue of understanding the interaction between El Niño and the time-mean climate. The recent study by Sun (2003), Sun et al. (2004), and Sun (2004) suggest that ENSO behaves as a heat-pump that regulates the time-mean climate of the tropical Pacific. If ENSO in the models is not right, the time-mean SST is unlikely right. Further study needs to delineate the role of the ocean feedback in maintaining the mean climate or equivalently how ENSO equilibrates with the time-mean climate of the tropical Pacific.

Underestimating the negative feedbacks in the central equatorial Pacific does not suggest that the models overestimate global warming. The NCAR coupled model—the NCAR CCSM-- has been found to have a lower sensitivity to increased $CO_2$ forcing than the GFDL coupled model (Jeff Kiehl, personal communication). Averaged globally, the feedback from shallow boundary layer clouds in regions outside the equatorial Pacific may weigh heavily in determining the total feedback of clouds. Also, the forcing due to increases in $CO_2$ is also not the same as the El Niño

warming. Nonetheless, our confidence with the model predictions of global warming may have to come from how well the model simulate the feedbacks on the shorter time-scales because it is over these time-scales we have better data and know more quantitatively the feedbacks in Nature.

.

## References:


Anderson, J. L., V. Balaji, A. J. Broccoli, W. F. Cooke, T. L. Delworth, K. W. Dixon, L. J. Donner, K. A. Dunne, S. M. Freidenreich, S. T. Garner, R. G. Gudgel, C.T. Gordon, I. M. Held, R. S. Hemler, L. W. Horowitz, S. A. Klein, T. R. Knutson, P. J. Kushner, A. R. Langenhorst, N.-C. Lau, Z. Liang, S. L. Malyshev, P. C. D., Milly, M. J. Nath, J. J. Ploshay, V. Ramaswamy, M. D. Schwarzkopf, E. Shevliakova, J. J. Sirutis, B. J. Soden, W. F. Stern, L. A. Thompson, R. John Wilson, A. T. Wittenberg, and B. L. Wyman, 2004: The new GFDL global atmosphere and land model AM2/LM2: Evaluation with prescribed SST simulations. *J. Climate*, accepted.

Barkstrom, B.R., E.F. Harrison, G.L. Smith, R. Green, J. Kibler, R.D. Cess, and the ERBE Science Team, 1989: Earth Radiation Budget Experiment (ERBE) Archive and April 1985 Results. *Bull. Amer. Meteror. Soc.,* 70, 1254-1262.

Cess, R. D., and G. L. Potter, 1988: A methodology for understanding and intercomparing atmospheric climate feedback processes in general circulation models. J. Geophys. Res., 93, 8305–8314.

Collins, W. D., J. J. Hack, B. A. Boville, P. J. Rasch, D. L. Williamson, J. T. Kiehl, B. Briegleb, J. R. McCaa, C. Bitz, S.-J. Lin, R. B. Rood, M. Zhang, and Y. Dai, 2003: Description of the NCAR Community Atmosphere Model (CAM2). 171pp. [Available online at http://www.ccsm.ucar.edu/models/atm-cam/docs/cam2.0/description.pdf.]

Collins, W. D., P. J. Rasch, B. A. Boville, J. J. Hack, J. R. McCaa, D. L. Williamson, J. T. Kiehl, B. Briegleb, C. Bitz, S.-J. Lin, M. Zhang, and Y. Dai, 2004: Description of the NCAR Community Atmosphere Model (CAM 3.0), Technical Report NCAR/TN-464+STR,

National Center for Atmospheric Research, Boulder, Colorado, 210 pp.

Chou, M.-D., and M.J., Suarez, 1996: A Solar Radiation Parameterization (CLIRAD-SW). NASA Technical Memorandum no. 104606, v. 15, 48 pp.

Collins, M., S.F.B. Tett, and C. Cooper, 2001: The internal climate variability of a HadCM3, a version of the Hadley Centre coupled model without flux adjustments. *Clim. Dyn.,* 17: 61-81.

Fu, R., DelGenio, A.D., Rossow, W.B., and Liu, W.T., 1990: Cirrus cloud thermostat for tropical sea surface temperature tested using satellite data. *Nature*, 358, 394-397.

Gregory, D., 1990: Convection scheme. Unified Model Documentation Paper No. 27, United Kingdom Meteorological Office, Bracknell, Berkshire RG122SZ, UK.

Gregory, D., and P.R.R. Rowntree, 1990: A mass flux convection scheme with representation of cloud ensemble characteristics and stability dependent closure. Mon. Wea. Rev., 118, 1483-1506.

Hack, J. J., 1994: Parameterization of moist convection in the National Center for Atmospheric Research Community Climate Model (CCM2). *J. Geophys. Res.,* **99**, 5551-5568.

Ingram, W.J., 2002: On the Robustness of the Water Vapor Feedback: GCM Vertical Resolution and Formulation. *J. Climate*, 11, 1131-1149.

Kiehl, J., J. J. Hack, G. Bonan, B. A. Boville, D. Williamson, and P. J. Rasch, 1998: The National Center for Atmospheric Research Community Climate Model: CCM3. *J. Climate*, 11, 1131-1149.

Liu, W. T., 2002: Progress in scatterometer applications. *J. Oceanogr*., 58, 121–136.

Lock, A. P., A. R. Brown, M. R. Bush, G. M. Martin, and R. N. B. Smith, 2000: A new boundary layer mixing scheme. Part I: Scheme description and single-column model tests. Mon. Wea. Rev., 128, 3187-3199.

Mellor, G.L., and T. Yamada, 1974: A hierarchy of turbulence closure models for planetary boundary layers, *J. Atmos. Sci*. ,**31**, 1791-1806.

Moorthi, S. and M. Suarez, 1992: Relaxed Arakawa-Schubert: a parameterization of moist convection for general circulation models. Mon. Wea. Rev., 120, 978-1002.

Murtugudde, R., J. Beauchamp, C. R. McClain, and A. J. Busalacchi, 2002: Effects of penetrative radiation on the upper tropical ocean circulation. *J. Climate*, 15, 470-496.

Pierrehumbert, R. T., 1995: Thermostats, radiator Fins, and the local runaway greenhouse. *J. Atmos. Sci.,* 52, 1784-1806.

Ramanathan, V. and W. Collins, 1991: Thermodynamic regulation of ocean warming by cirrus clouds deduced from observations of the 1987 El Niño. *Nature*, 351, 27-32.

Soden, B., A.J. Broccoli, and R.S. Hemler, 2004: On the Use of Cloud Forcing to Estimate Cloud Feedbacks. *J. Climate*, **17**, 185-205.

Stockdale, T.N., A.J. Busalacchi, D.E. Harrison, and Richard Seager, 1998: Ocean Modeling for ENSO. *J. Geophys. Res.,* 103, 14,325-14,355.

Suarez, M.J., 1995: Documentation of the ARIES/GEOS Dynamical Core, version 2. NASA Technical Memorandum no. 104606, v. 5, 53 pp

Sun, D.-Z., 2004: The Control of Meridional Differential Heating Over the Level of ENSO activity: A Heat-Pump Hypothesis. Accepted for publication in *Ocean-Atmosphere Interaction and Climate Variability*, AGU Geophysical Monograph, Edited by C. Wang, S.-P. Xie, and J. Carton.

Sun, D.-Z., 2003:A Possible Effect of An Increase in the Warm-pool SST on the Magnitude of El Niño Warming *J. Climate*, **16**, 185-205.

Sun, D.-Z., 2000: The heat sinks and sources of the 1986-87 El Niño. *J. Climate*, **13**, 3533-3550.

Sun, D.-Z., C. Covey, and R.S. Lindzen, 2001: Vertical correlations of water vapor in GCMs. *Geophys. Res. Lett.*, **28** , 259-262.

Sun, D.-Z. and Z. Liu, 1996: Dynamic ocean-atmosphere coupling: a thermostat for the tropics. *Science,* 272, 1148-1150.

Sun, D.-Z., J. Fasullo, T. Zhang, and A. Roubicek, 2003: On the radiative and dynamical feedbacks over the equatorial Pacific cold-tongue. *J. Climate.*, **16,** 2425—2432.

Sun, D.-Z., and I. Held, 1996: A comparison of modeled and observed relationships between interannual variations of water vapor and temperature. *J. Climate*, **9**, 665-675.

Sun. D.-Z. and K. E. Trenberth, 1998: Coordinated heat removal from the tropical Pacific region during the 1986-87 El Niño. *Geophys. Res. Lett.,* 25, 2659-2662.

Sun, D.-Z., T. Zhang, and S.-I. Shin, 2004 : The effect of subtropical cooling on the amplitude of ENSO: a numerical study. *J. Climate*, **17**, 3786-3798.

Trenberth, K.E., J.M. Caron, and D.P. Stepaniak, 2001: The atmospheric energy budget and implications for surface fluxes and ocean heat transport. *Climate Dyn*., **17**, 259-296.

Wallace, J.M., 1992: Effect of deep convection on the regulation of tropical sea surface temperature. *Nature*, 357, 230-231

Wetherald, R. T., and S. Manabe, 1988: Cloud feedback processes in a general circulation model. J. Atmos. Sci., 45, 1397–1415.

Xie, P., and P.A. Arkin, 1996: Analyses of Global Monthly Precipitation Using Gauge Observations, Satellite Estimates, and Numerical Model Predictions. *J. Climate,* **9**, 840-858.

Yanai, M., S. Esbensen, and J.-H., Chu, 1973: Determination of bulk properties of tropical cloud clusters from large-scale heat and moisture budgets. J. Atmos. Sci., 30, 611-627.

Zhang, G.J., and N. A. McFarlane, 1995: Sensitivity of climate simulations to the

parameterization of cumulus convection in the Canadian Climate Centre general circulation model. *Atmos.-Ocean*, **33**, 407-446.

Acknowledgments

This research was supported partially by NOAA's office of global programs and partially by the NSF climate dynamics program (ATM-9912434 and ATM-0331760).The leading author (D.-Z. Sun) would like to thank Prof. Robert Dickinson for his encouraging comments.

This work was performed under the auspices of the U.S. Department of Energy by University of California, Lawrence Livermore National Laboratory under Contract W-7405-Eng-48.

## Table Legends

Table 1: Atmospheric feedbacks over the equatorial Pacific (5ºS-5ºN, 150ºE-270ºE) from leading climate models. See text for the definition of the symbols for the various feedbacks. The values for these feedbacks were obtained through a linear regression using the interannual variations of the SST and the corresponding fluxes over the equatorial Pacific.

## Figure Legends

Figure 1: Tropical Pacific SST from observations and seven coupled climate models. Shown are annual mean conditions. The atmospheric components of the seven coupled models are respectively the NCAR CAM1, the NCAR CAM2, the NCAR CAM3, the NASA NSIPP GCM, the Hadely Centre model, the GFDL AM2p10, and the GFDL AM2p12.

Figure 2: Response of the greenhoue effect of water vapor ($G_a$) to El Niño warming. Show are regression coefficents and they are obtained by linearly regressing the greenhouse effect of water vapor at each grid point on the SST averaged over the equatorial Pacific ($5^oS$-$5^oN$, $150^oE$-$250^oE$). The interannual variations of $G_a$ over the ERBE period are used for the calculations.

Figure 3: Response of the greenhouse effect of clouds ($C_l$) to El Niño warming. Show are regression coefficents and they are obtained by linearly regressing the greenhouse effect of clouds at each grid point on the SST averaged over the equatorial Pacific ($5^oS$-$5^oN$, $150^oE$-$250^oE$). The interannual variations of the concerned quantities over the ERBE period are used for the calculations.

Figure 4: Response of the shortwave forcing of clouds ($C_s$) to El Niño warming. Show are regression coefficents and they are obtained by linearly regressing the short-wave forcing of clouds at each grid point on the SST averaged over the equatorial Pacific ($5^oS$-$5^oN$, $150^oE$-$250^oE$). The interannual variations of the concerned quantities over the ERBE period are used for the calculations.

Figure 5: Response of the precipitation to El Niño warming. Show are regression coefficents and they are obtained by linearly regressing the precipitation at each grid point on the SST averaged over the equatorial Pacific ($5^oS$-$5^oN$, $150^oE$-$250^oE$). The interannual variations of the concerned quantities over the ERBE period are used for the calculations. The precipitation data are from Xie and Arkin (1996).

Figure 6: Response of the convergence of vertically integerated transport of energy by the atmospheric circulations ($D_a$) to El Niño warming. Show are regression coefficents and they are obtained by linearly regressing the value of $D_a$ at each grid point on the SST averaged over the equatorial Pacific ($5^oS$-$5^oN$, $150^oE$-$250^oE$). The interannual variations of the concerned quantities over the ERBE period are used for the calculations.

Figure 7: Response of the net surface heating ($F_s$) to El Niño warming. Show are regression coefficents and they are obtained by linearly regressing the net surface heating at each grid point on the SST averaged over the equatorial Pacific ($5^oS$-$5^oN$, $150^oE$-$250^oE$). The interannual variations of the concerned quantities over the ERBE period are used for the calculations. The data used for Fs are the same as in Sun et al. (2003).

Table 1

**Atmospheric Feedbacks in Models and Observations**

| Name of Process | Feedback ($Wm^{-2}K^{-1}$) | | | | | | | |
|---|---|---|---|---|---|---|---|---|
| | Observation | NCAR/CAM1 | NCAR/CAM2 | NCAR/CAM3 | NASA/NSIPP-1 | ukmo-98a | GFDL/AM2p10 | GFDL/AM2p12 |
| $\frac{\partial(G_a)}{\partial T}$ | 6.72 ± 0.27 | 9.10 ± 0.43 | 8.39 ± 0.41 | 8.89 ± 0.39 | 8.21 ± 0.33 | 10.10 ± 0.48 | 8.08 ± 0.33 | 9.43 ± 0.32 |
| $\frac{\partial(C_L)}{\partial T}$ | 12.21 ± 1.03 | 15.94 ± 1.35 | 6.64 ± 0.63 | 7.21 ± 0.72 | 9.14 ± 0.72 | 7.63 ± 0.86 | 13.52 ± 0.78 | 14.74 ± 0.96 |
| $\frac{\partial(C_S)}{\partial T}$ | -10.93 ± 1.37 | -4.98 ± 0.60 | 1.87 ± 0.96 | -0.56 ± 0.78 | -5.95 ± 0.77 | -8.94 ± 1.33 | -12.74 ± 0.79 | -12.58 ± 1.09 |
| $\frac{\partial(D_a)}{\partial T}$ | -16.69 ± 1.51 | -13.63 ± 1.76 | -9.18 ± 1.40 | -9.02 ± 1.20 | -14.08 ± 0.96 | -12.11 ± 1.53 | -17.63 ± 0.92 | -19.40 ± 1.28 |
| $\frac{\partial(F_A)^*}{\partial T}$ | -8.69 ± 1.76 | 6.42 ± 1.24 | 7.72 ± 1.12 | 6.53 ± 1.00 | -2.69 ± 0.97 | -3.33 ± 1.64 | -8.77 ± 1.12 | -7.81 ± 1.53 |
| $\frac{\partial(F_S)}{\partial T}$ | -14.89 ± 1.83 | 0.44 ± 1.24 | 1.48 ± 1.13 | 0.30 ± 1.02 | -8.71 ± 0.98 | -9.15 ± 1.64 | -14.73 ± 1.13 | -13.80 ± 1.53 |

The net atmospheric feedback $\frac{\partial(F_A)}{\partial T} = \frac{\partial(G_a)}{\partial T} + \frac{\partial(C_L)}{\partial T} + \frac{\partial(C_S)}{\partial T} + \frac{\partial(D_a)}{\partial T}$

**Table 1**

Fig. 1

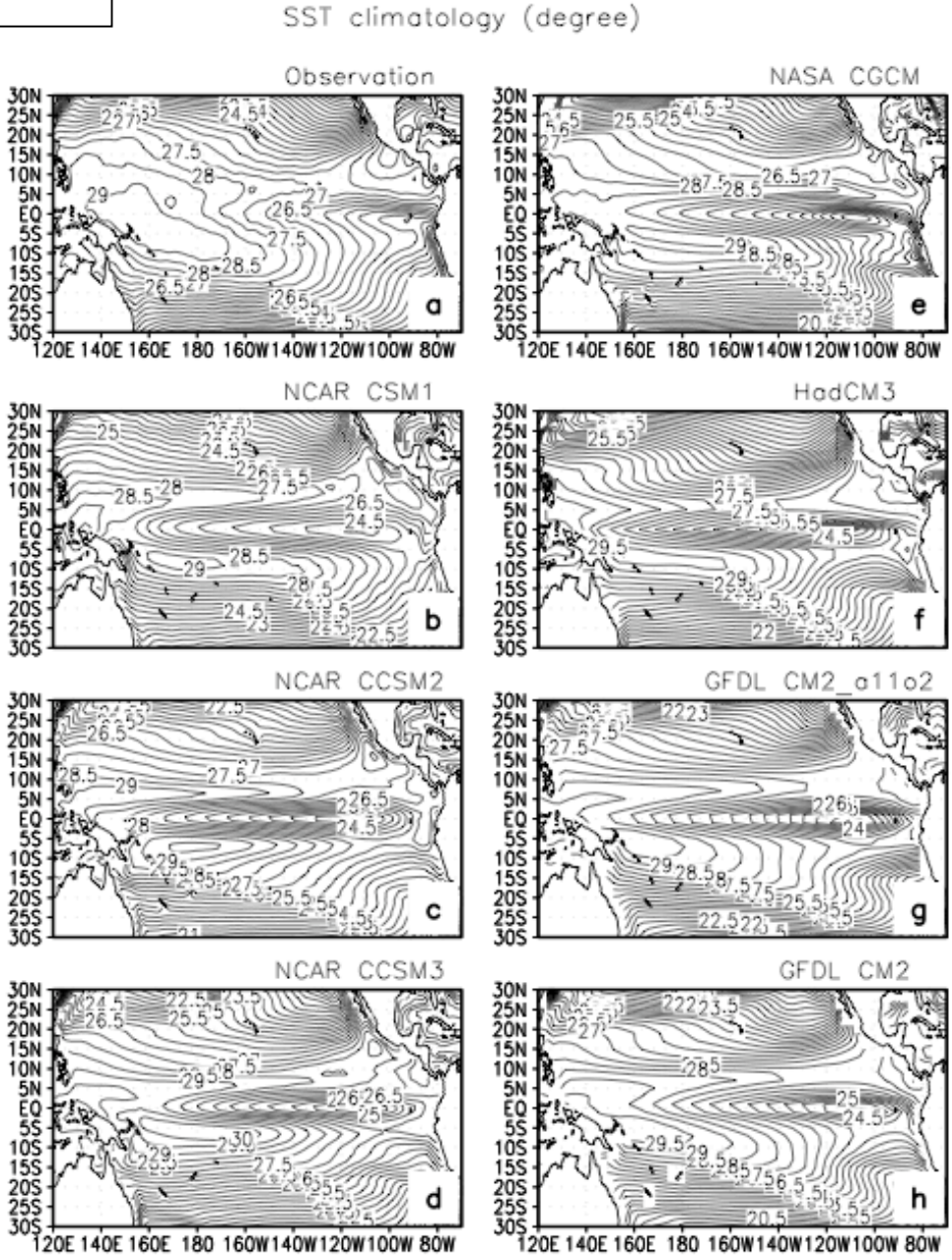
SST climatology (degree)
Observation
NASA CGCM
NCAR CSM1
HadCM3
NCAR CCSM2
GFDL CM2_a11o2
NCAR CCSM3
GFDL CM2
a
b
c
d
e
f
g
h
30N 25N 20N 15N 10N 5N EQ 5S 10S 15S 20S 25S 30S
120E 140E 160E 180 160W 140W 120W 100W 80W

Fig.1

Fig. 2

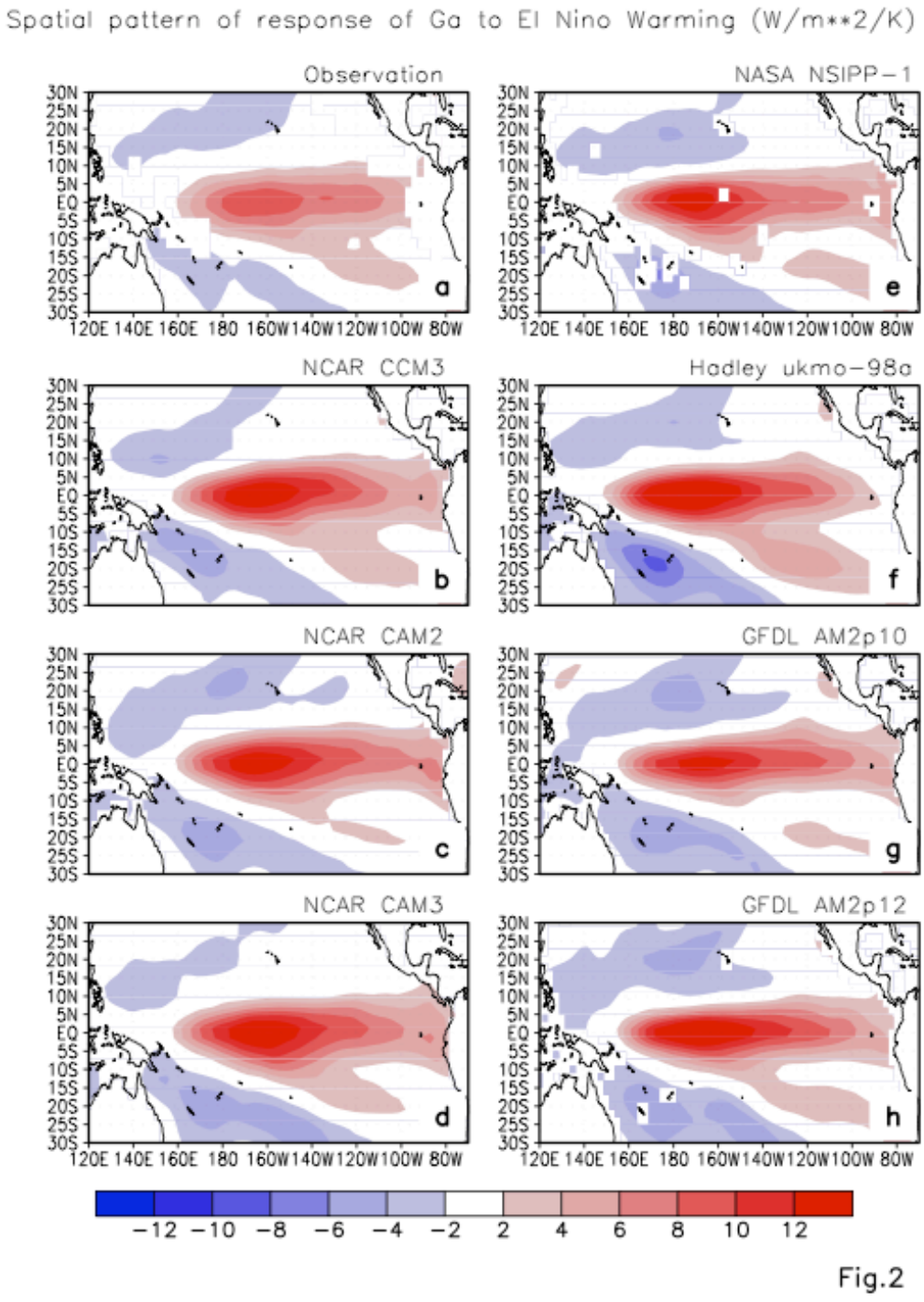
Spatial pattern of response of Ga to El Nino Warming (W/m**2/K)
Observation
NASA NSIPP-1
NCAR CCM3
Hadley ukmo-98a
NCAR CAM2
GFDL AM2p10
NCAR CAM3
GFDL AM2p12
a
b
c
d
e
f
g
h
30N 25N 20N 15N 10N 5N EQ 5S 10S 15S 20S 25S 30S
120E 140E 160E 180 160W 140W 120W 100W 80W
−12 −10 −8 −6 −4 −2 2 4 6 8 10 12

Fig.2

Fig. 3

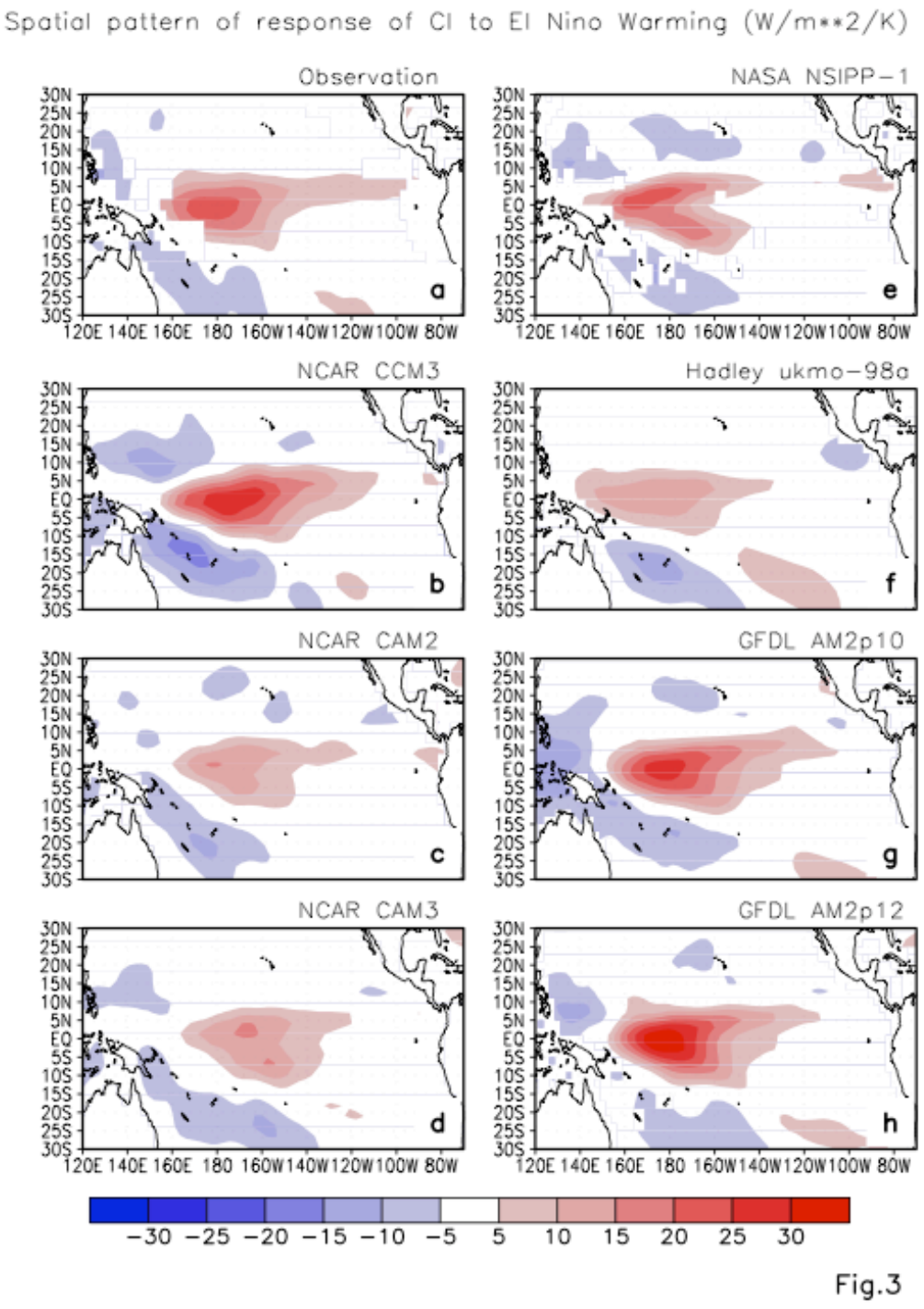
Spatial pattern of response of CI to El Nino Warming (W/m**2/K)
Observation
NASA NSIPP-1
NCAR CCM3
Hadley ukmo-98a
NCAR CAM2
GFDL AM2p10
NCAR CAM3
GFDL AM2p12
a
b
c
d
e
f
g
h
30N 25N 20N 15N 10N 5N EQ 5S 10S 15S 20S 25S 30S
120E 140E 160E 180 160W 140W 120W 100W 80W
-30 -25 -20 -15 -10 -5 5 10 15 20 25 30

Fig.3

Fig. 4

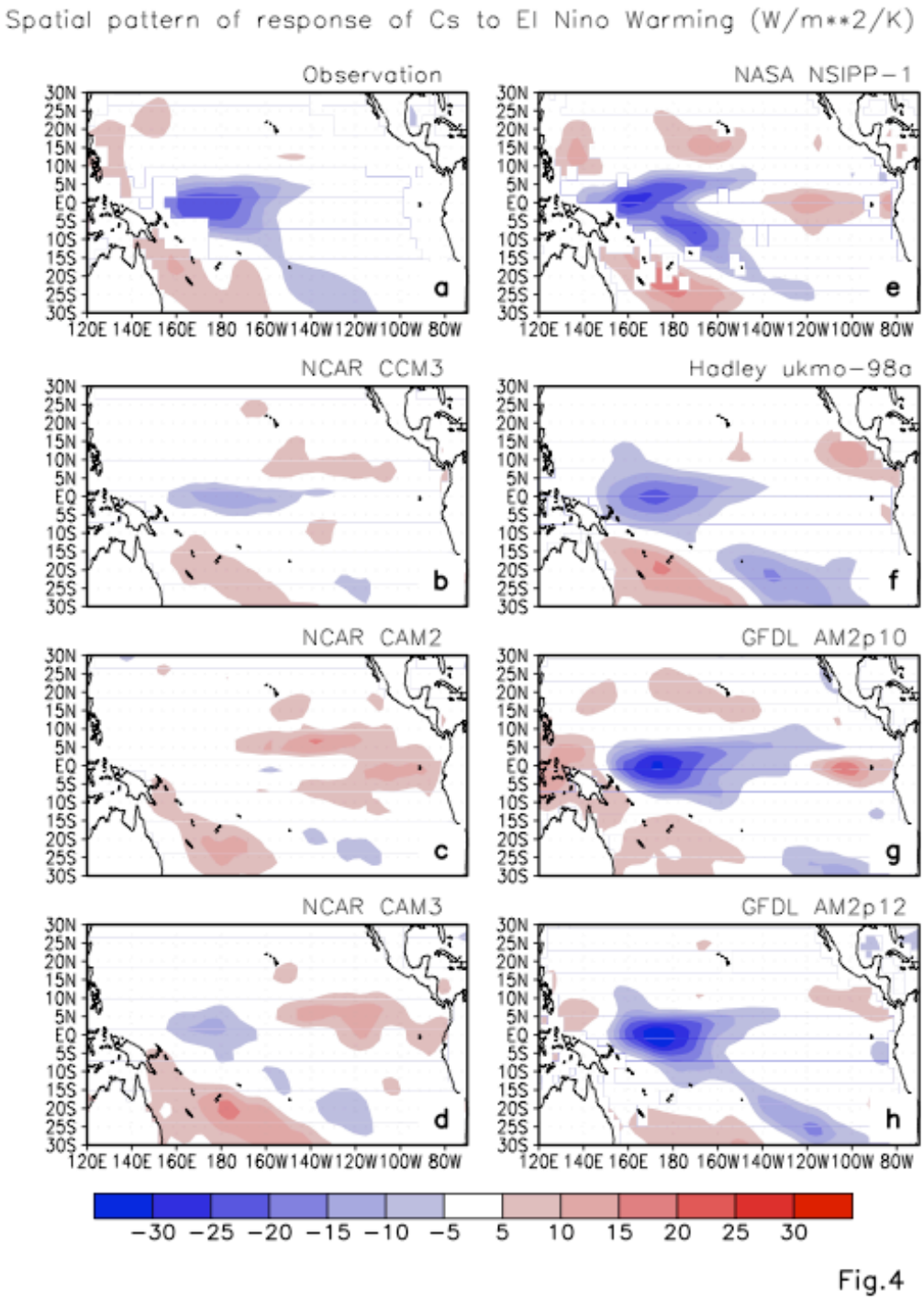
Spatial pattern of response of Cs to El Nino Warming (W/m**2/K)
Observation
NASA NSIPP-1
NCAR CCM3
Hadley ukmo-98a
NCAR CAM2
GFDL AM2p10
NCAR CAM3
GFDL AM2p12
a
b
c
d
e
f
g
h
30N 25N 20N 15N 10N 5N EQ 5S 10S 15S 20S 25S 30S
120E 140E 160E 180 160W 140W 120W 100W 80W
-30 -25 -20 -15 -10 -5 5 10 15 20 25 30

Fig.4

Fig. 5

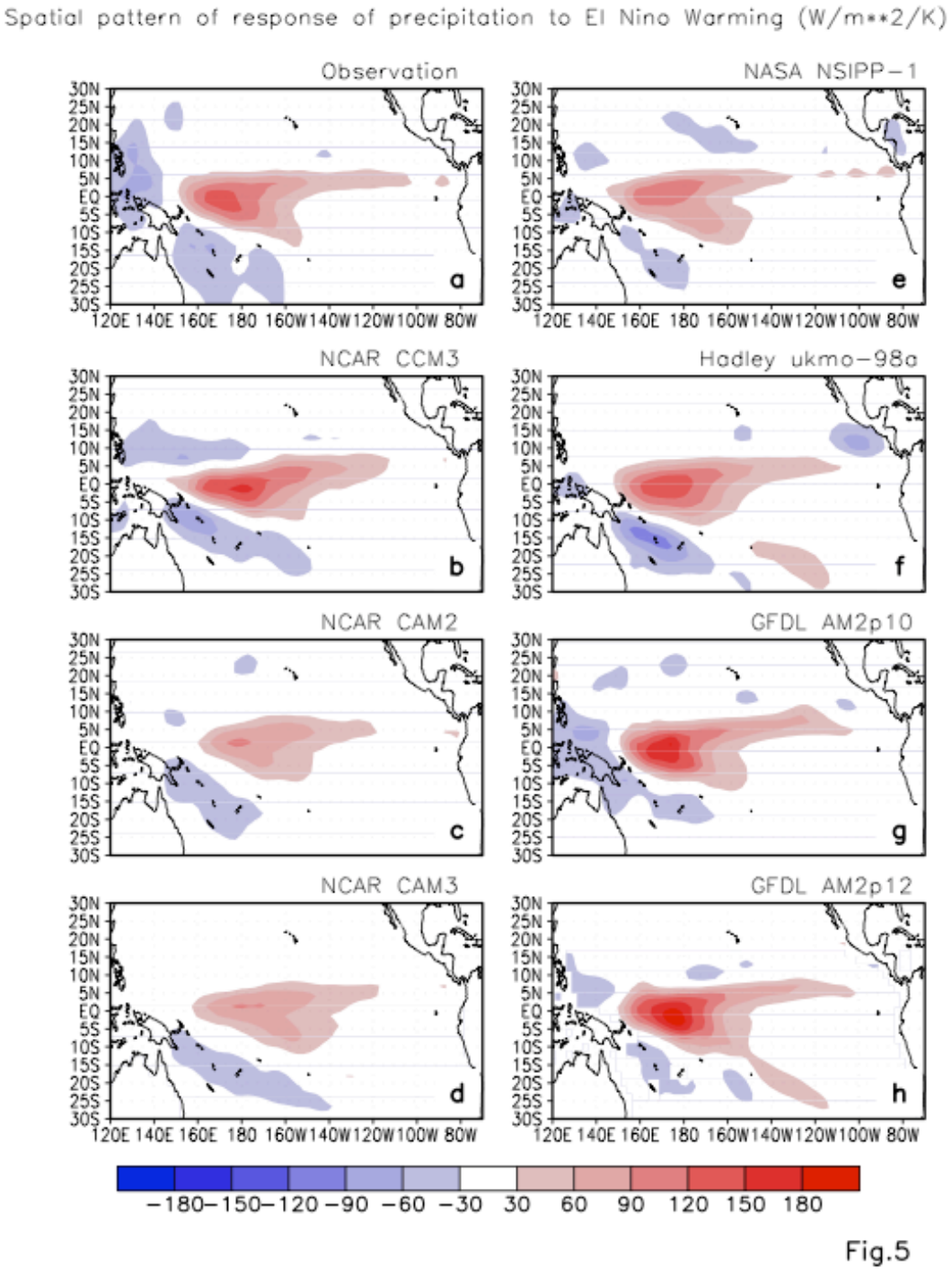
Spatial pattern of response of precipitation to El Nino Warming (W/m**2/K)
Observation
NASA NSIPP-1
NCAR CCM3
Hadley ukmo-98a
NCAR CAM2
GFDL AM2p10
NCAR CAM3
GFDL AM2p12
a
b
c
d
e
f
g
h
30N 25N 20N 15N 10N 5N EQ 5S 10S 15S 20S 25S 30S
120E 140E 160E 180 160W 140W 120W 100W 80W
-180 -150 -120 -90 -60 -30 30 60 90 120 150 180

Fig.5

Fig.6

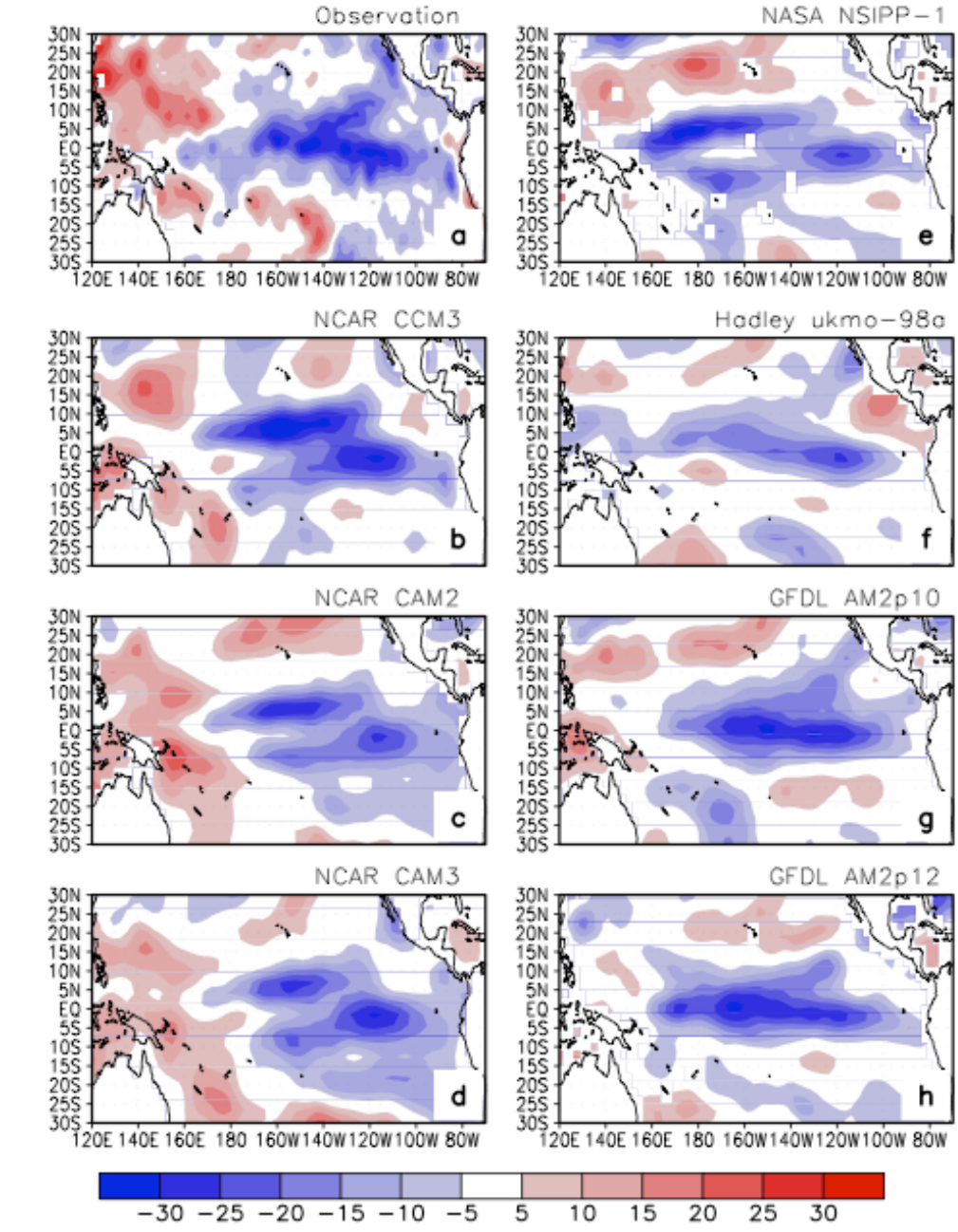
Spatial pattern of response of Da to El Nino Warming (W/m**2/K)
Observation
NASA NSIPP-1
NCAR CCM3
Hadley ukmo-98a
NCAR CAM2
GFDL AM2p10
NCAR CAM3
GFDL AM2p12
a
b
c
d
e
f
g
h
30N 25N 20N 15N 10N 5N EQ 5S 10S 15S 20S 25S 30S
120E 140E 160E 180 160W 140W 120W 100W 80W
-30 -25 -20 -15 -10 -5 5 10 15 20 25 30

Fig.6

Fig. 7

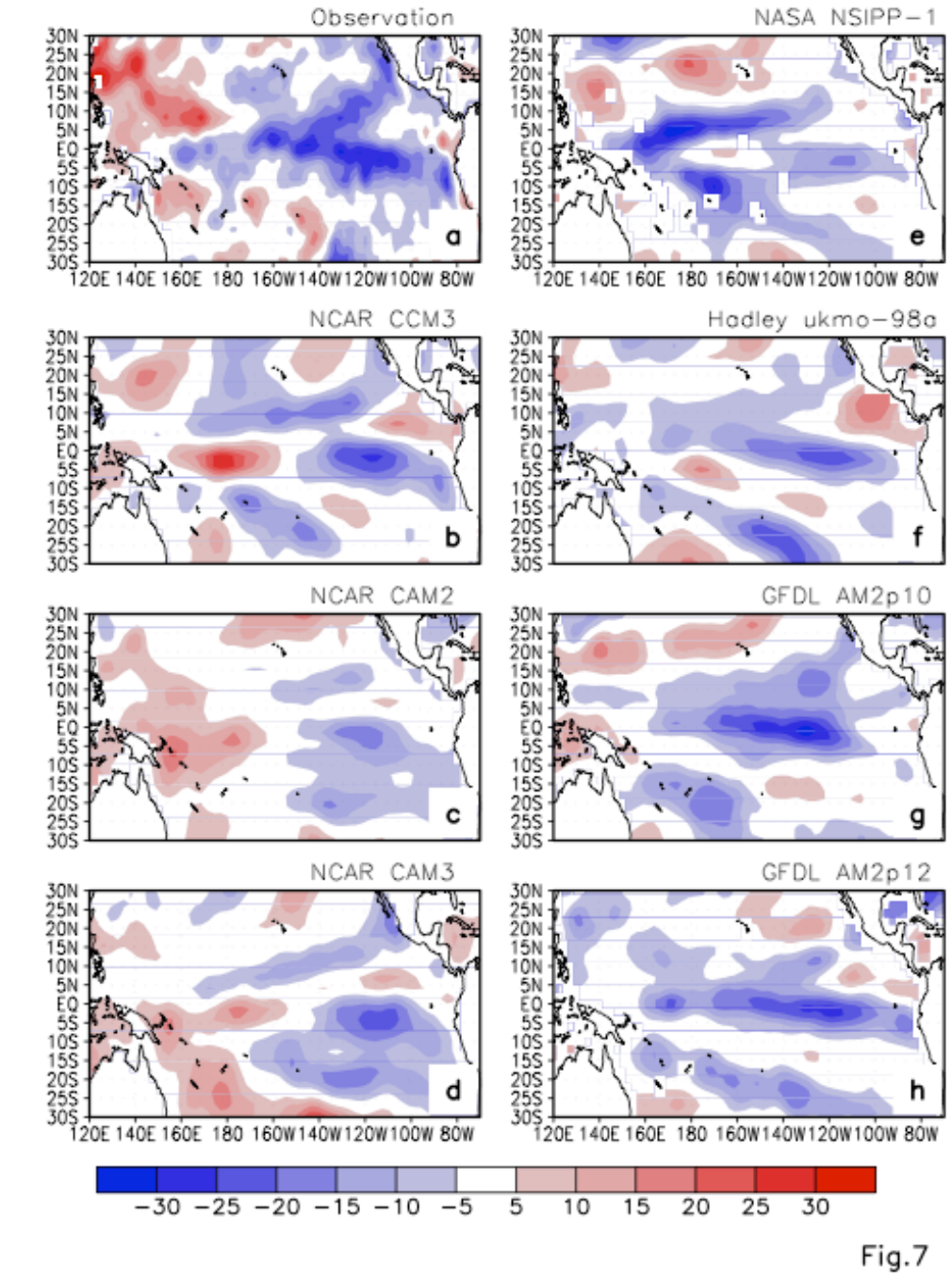
Spatial pattern of response of Fs to El Nino Warming (W/m**2/K)
Observation
NASA NSIPP-1
NCAR CCM3
Hadley ukmo-98a
NCAR CAM2
GFDL AM2p10
NCAR CAM3
GFDL AM2p12
a
b
c
d
e
f
g
h
30N 25N 20N 15N 10N 5N EQ 5S 10S 15S 20S 25S 30S
120E 140E 160E 180 160W 140W 120W 100W 80W
-30 -25 -20 -15 -10 -5 5 10 15 20 25 30

Fig.7